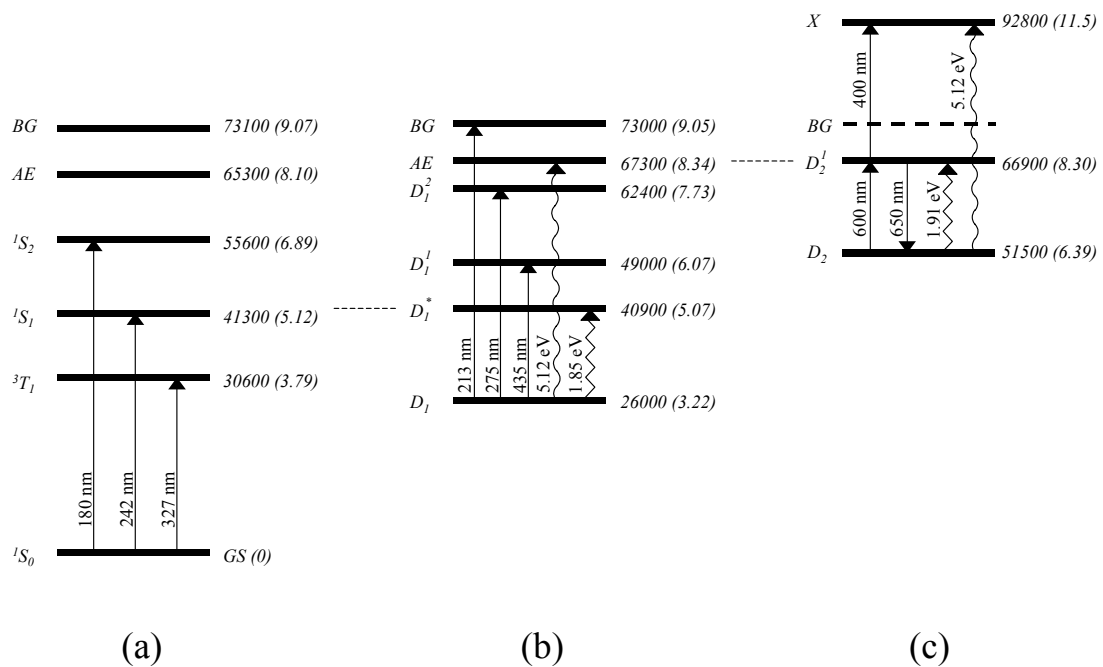


## Bragg Gratings White Paper



Authored by Martin Kristensen

Presented by Ibsen Photonics

## Table of Contents

Fundamentals of photosensitivity in germanium-doped silica .....	3
Introduction.....	3
Detailed theoretical predictions of photosensitivity and UV-induced effects .....	4
Performance of the model.....	7
Discussion and conclusion.....	9
Phenomenology of grating writing – practical aspects .....	11
Fabrication methods for fibre Bragg gratings.....	15
Phase mask dither method .....	15
Polarisation-control method.....	15
Grating applications .....	20
Simple filters.....	20
Advanced filters.....	20
Add drop multiplexers .....	22
DFB fibre lasers .....	25
Strong gratings .....	30
Thermal stability of gratings.....	31
References.....	33

## Fundamentals of photosensitivity in germanium-doped silica

### *Introduction*

Since the discovery of light-induced refractive index changes in silica materials [1] and the invention of the side-writing method [2], UV-writing of gratings in optical fibres has become an important technological field for telecommunications and optical sensors. However, the fundamental understanding of the UV-induced processes in glass materials has lagged far behind the technological development.

In brief, there are two competing classes of models for UV-induced index changes in germanium-doped silica. Microscopic models are based on the assumption that defects formed in the glass lead to a higher refractive index [3-8]. A large number of defects have been identified using different spectroscopic methods and theoretical calculations. However, no satisfactory quantitative agreement had until recently been found with experimentally observed index changes. The second class of models is based on macroscopic changes in the glass [9-12]. In these models it is assumed that the UV-light induces compaction or stress changes in the glass leading to refractive index changes. In some cases good qualitative agreement is found with experimental results, but there seem to be problems establishing a general quantitative agreement. In addition, a macroscopic model lacks the ability to explain what happens on the microscopic level and thereby in most cases also the ability to give predictions about how to improve the base materials. It is therefore desirable to have a complete microscopic understanding.

The confusing picture is largely due to the great complexity of glass material. It can almost be characterised as the theoretician's nightmare. This is partly due to the amorphous structure, partly due to the additional complications related to doping of the pure silica material, and partly due to the great experimental difficulties associated with precise spectroscopic investigations in the deep-UV part of the spectrum where the most important changes take place. Even though many researchers tend to agree that a large part of the UV-induced refractive index changes must be linked to some kind of compaction of the glass, there is still a lot of controversy on the details. For instance there is absolutely no consensus on how large a fraction of the refractive index change can be related to absorption changes and how much is simply compaction.

Another interesting aspect of glass is that there are fundamental problems related to the transition from the microscopic world to the macroscopic world. For instance a compaction of the structure must be related somehow to microscopic changes. Is it just a smooth and evenly distributed reduction of all bond lengths, or do the bond angles also change, - or does the change predominantly take place at specific locations? These kinds of questions are indeed more easily answered in crystalline materials using techniques such as X-ray diffraction.

### ***Detailed theoretical predictions of photosensitivity and UV-induced effects using the dipole-quadrupole model parameterisation***

Most models for UV photosensitivity do not allow detailed predictions of the outcome of experiments. One of the few exceptions is a model based on parameterisation of the microscopic interactions in germanium-doped silica [8].

Two of the most important parameters for UV-induced index changes are the UV-sensitivity and the stability of the induced changes. A large number of publications discuss how to increase the UV-sensitivity of glasses, but there is no consensus on what UV-sensitivity really is. The reason is probably that in most cases the amount of UV-induced index change depends on several parameters such as wavelength, power level, fluence and polarisation of the UV-light, and temperature and previous treatment of the sample with e.g. hydrogen. The dependencies on fluence and loading are the best studied, because of their commercial importance. The index change is not a simple, linear function of fluence, but rather a complicated curve, which does not allow a straightforward definition of the UV-sensitivity. Concerning treatment of the samples with hydrogen or deuterium there is consensus that it increases the UV-sensitivity.

The other important aspect of UV-induced processes in glass is the decay of the refractive index changes. As commercial products based on UV-writing find increasing applications in telecommunications and as optical sensors, accelerated ageing tests have been performed to determine their stability. Most of the results are analysed using a model that assumes the index changes are due to a very broad spectrum of defects with activation energies from 0.5eV to 3.5eV [13,14]. However, only very few researchers have discussed whether such a broad smooth spectrum is physically reasonable and only limited work has been done to relate the annealing results to the models for UV-induced processes.

The model, which allows the most detailed predictions [8,15], is based on the assumption that germanium sites in the glass work as gates for the transfer of energy from the light to the glass matrix. When a germanium site has absorbed a photon, the energy may be transferred to other sites in the glass leading to rearrangement of the local structure. The energy transfer happens predominantly through dipole-quadrupole transitions, leading to an  $r^{-8}$  dependence of the transition probability as a function of the distance,  $r$ , from the germanium site [16,17]. In addition, some multi-photon processes are possible using the excited germanium site as intermediate level. It is assumed that two different metastable defect states are formed in the silica matrix. Formation of the first type (or class) of defect,  $D_1$ , in the glass increases the refractive index because it is situated higher in the bandgap bringing its fundamental transitions closer to visible wavelengths. On the other hand, formation of another type of defect,  $D_2$ , with very small overlap integral to electronic states above the bandgap reduces the refractive index, since transitions from these states to more normal electronic glass states are practically forbidden.

It is important to emphasise that the two defects discussed above may not exclusively be two very specific defects. Probably they just represent two classes of defects with average properties like these two ‘model defects’. In addition, the refractive index

changes ascribed to the defects may be partly due to density changes related to the presence of the defects.

It is possible to include results for sensitised glass by assuming that sensitisation has a catalytic effect, which leads to increased absorption near 242nm and to reduced steric hindrance of some of the induced processes in the glass. Finally, it is possible to use the model to achieve quantitative agreement with anneal-experiments performed on gratings in different fibres and to extract activation energies and trial rates for thermal elimination of the two types of UV-induced defects. Activation energies ( $1.85 \pm 0.15 \text{ eV}$  and  $1.91 \pm 0.15 \text{ eV}$ ) and rates ( $(2.7 \pm 1.9) \times 10^{13} \text{ Hz}$  and  $(7.2 \pm 4.5) \times 10^{13} \text{ Hz}$ ) are determined for thermal elimination of the defect states contributing to the refractive index change.

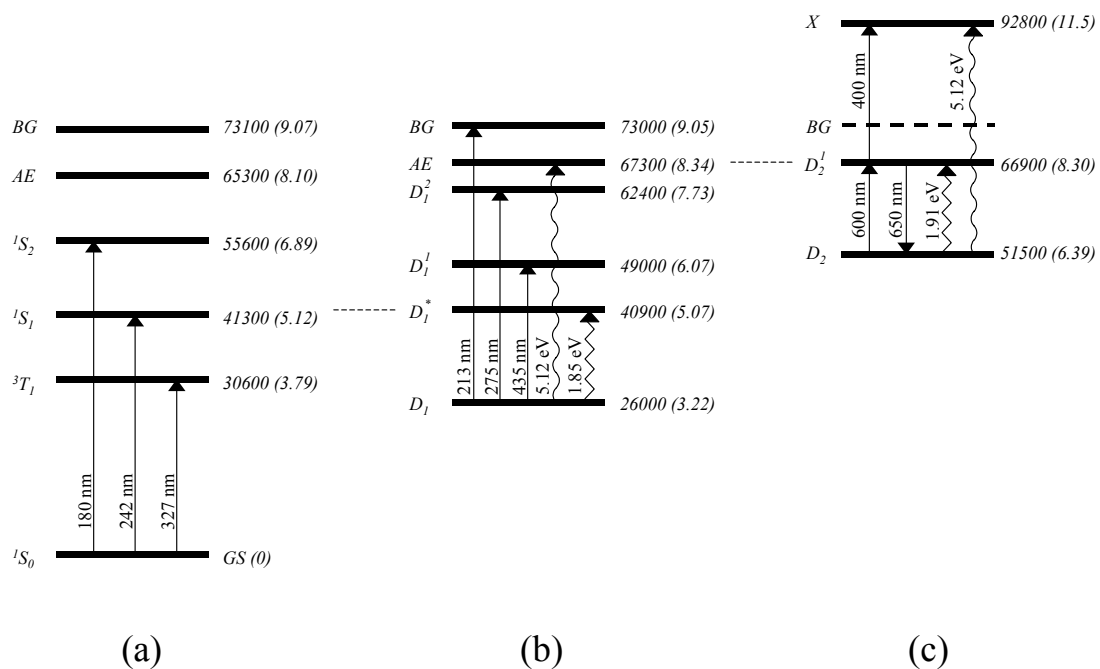


Fig. 1. Energy level scheme for the germanium sites (a) and the defects  $D_1$  (b) and  $D_2$  (c) involved in the UV-induced processes in silica glass [8]. Levels are drawn as horizontal lines with the energy in  $\text{cm}^{-1}$  and in parenthesis in electron volts (eV) to the right. Optical transitions are drawn as vertical lines labelled with the wavelength in nm. Non-radiative transitions are shown as vertical zigzag lines with the energy in eV. Absorption edges are labelled ‘AE’, bandgap energies labelled ‘BG’ and the ground state labelled ‘GS’. Dashed horizontal lines indicate transition states.  $X$  is a state localised above the bandgap and resonant with the singlet-triplet transition energy in the hydrogen molecule.

The most basic assumption of the model is that energy is initially absorbed in close vicinity of the germanium atoms and later transferred to other sites in the glass where defects are created. In this respect the model belongs to the class of microscopic models [3-7]. It is well known that germanium sites in silica have an absorption spectrum consisting of two strong singlet-singlet transitions near 242nm and 180nm [18]. The 242-nm absorption is strong for oxygen deficient germanium-doped silica

(e.g. with germanium-related oxygen deficient centres (GODC) such as two-coordinated germanium [19]). Most UV-writing is performed at wavelengths near the 242-nm absorption [20-22]. In Fig. 1 (a) these observations are collected in a simple level scheme for germanium sites with a ground state defined at  $0\text{cm}^{-1}$  and excited states at  $30600\text{cm}^{-1}$  ( $^3T_1$ ),  $41300\text{cm}^{-1}$  ( $^1S_1$ ) and  $55600\text{cm}^{-1}$  ( $^1S_2$ ). The states are broad due to phonon broadening and the existence of different germanium sites [5].

Based on the assumptions and assignments above it is possible to write down rate equations describing the UV-induced processes. Ideally these equations should describe all observations of UV-induced changes, both dynamic and static, and the thermal decay. In addition one may expect that they will agree with the observed optical luminescence during UV-writing and the induced changes in absorption. Finally, one may hope that they can predict new effects. The concentration of the index increasing defect,  $D_1$ , will be named  $x$  and the concentration of the index decreasing defect,  $D_2$ , will be named  $y$ . Assuming that  $y \ll x < 1$  it is possible to write simple rate equations for the defect concentrations at different positions in the glass:

$$\begin{aligned}\frac{dx}{dt} &= c_1(1-x) - c_2x \\ \frac{dy}{dt} &= c_3x - c_4y\end{aligned}\tag{1}$$

This gives the time dependence of the defect concentrations for each position in the glass. After finding expressions for  $c_1$ ,  $c_2$ ,  $c_3$  and  $c_4$  as a function of the distance from the nearest active germanium atom it will be possible to calculate the index change by integration over the germanium molar volume. We will spare you for these details, since they involve a lot of spectroscopy, chemistry and mathematics. This is all essential to get a good agreement with experimental data, but it is not important to understand the general properties of the model.

During the radial integration it is assumed that the distribution of germanium atoms is equidistant throughout the glass. This may not be entirely correct, but it is the simplest and most reasonable approximation. The result can formally be written

$$\Delta n \propto \int_0^{r_{\max}} \left[ \Delta n_{\max}^x x(r) + \Delta n_{\max}^y y(r) \right] \rho(r) r^2 dr\tag{2}$$

where  $\Delta n_{\max}^x$  is the index change induced by unit density of index increasing defects and  $\Delta n_{\max}^y$  is the index change induced by unit density of index decreasing defects. The radial density function,  $\rho(r)$ , is determined from experimental X-ray diffraction data for silica [23,24] starting at a silicon atom; e.g. the sum of the Si-Si and Si-O pair function distribution curves. This implies that the defect generation is considered to be equally likely at all atoms in the glass. There is no basic reason to make this assumption, but trial and error has shown that it is the only way to obtain good agreement with the experimental data. This becomes particularly obvious when considering the red luminescence curves and refractive index changes for very large

fluences or very high hydrogen loading pressures. In all these cases the experimental curves tend to show a step-like behaviour. It is almost impossible to imagine such behaviour could be due to something else than the radial distribution function. Particularly since the number of steps, their relative height and their position all agree perfectly with the properties of the radial distribution function.

For those who like to criticise the model for its many free parameters here is a real challenge. All these properties are largely independent of the details of the model. Whatever value of the free parameters one will get a qualitative behaviour like this. Of course the absolute properties do depend a lot on the parameters, but the qualitative features do not!

### ***Performance of the model***

Fig. 2 shows an example of the performance of the model in describing the red luminescence emitted during UV inscription. The absolute timing of the later steps is  $\sim 50\%$  off. Here may be room for some further improvement of the model parameters, but it should also be kept in mind that the deviation could perhaps also be due to difficulties with measuring the laser spot-size and keeping the laser alignment constant over long time intervals.

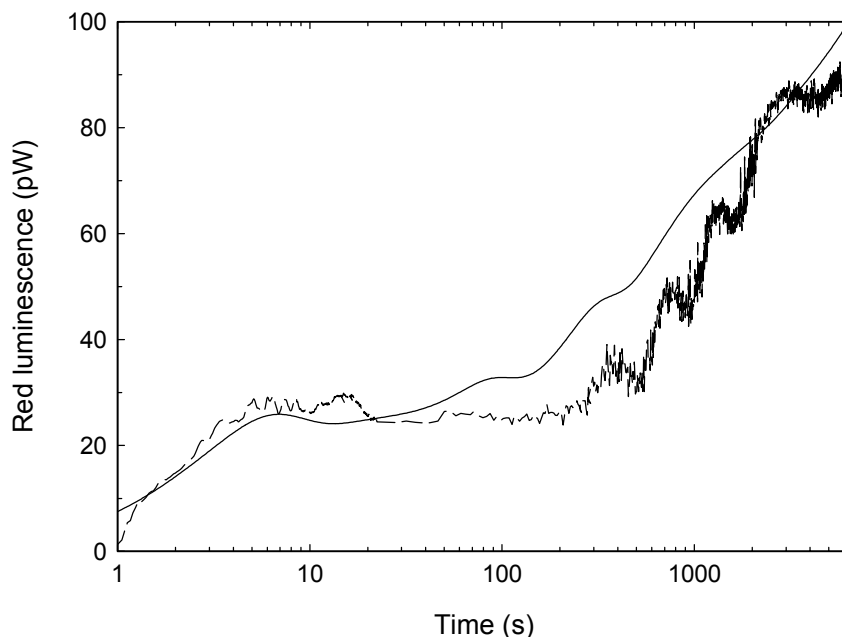


Fig. 2. The red luminescence measured with an optical spectrum analyser for a standard fibre with 3.2% germanium in the core during an exposure with the focused spot from a 244-nm frequency-doubled argon ion (FRED) laser [8,25,26]. The intensity is  $6\text{kW}/\text{cm}^2$  and the exposure length is  $40\mu\text{m}$ . The dashed, noisy line is the measured result and the full line is the prediction from the model. The relative time and height of the steps in the luminescence are reproduced well by the model even though the shape is rounded too much.

Another encouraging result is that the decay of the blue luminescence is well represented. It has been believed for several years that this decay follows a stretched exponential curve perhaps with an additional constant contribution [25,27]. This curve form indeed also gives a good fit to most spectra.

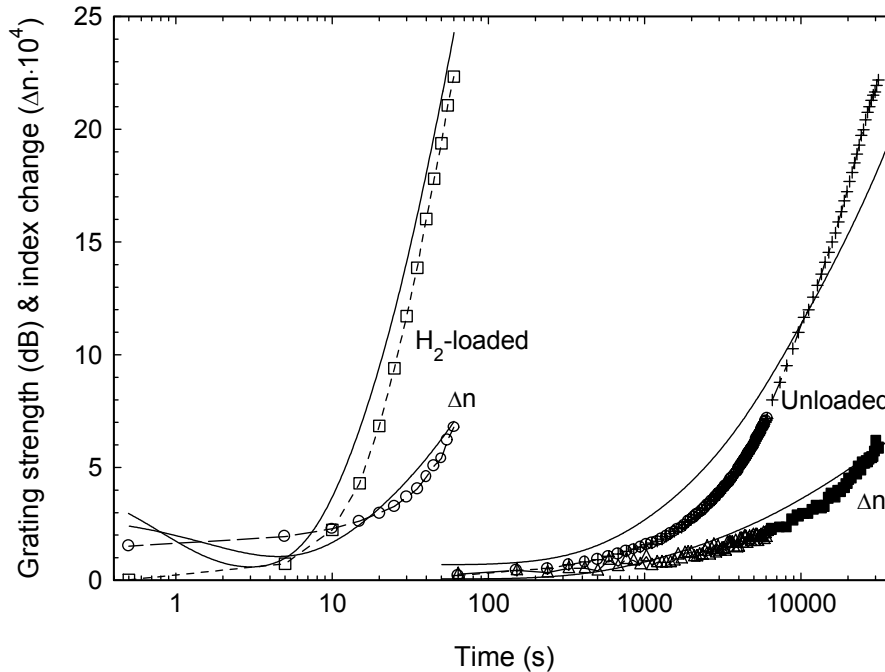


Fig. 3. Comparison of gratings written in the same 3.2% Ge-doped fibre at 244nm. The curves to the left represent the grating strength (dB) and effective refractive index change ( $\times 10^4$ ) obtained with 2.1%  $H_2$  loading [25]. Results to the right are obtained for the same fibre unloaded. Full drawn curves are the model predictions [15,28].

A more serious test of the model is if it is able to reproduce growth curves for the UV-induced refractive index. Fig. 3 shows some results for writing with a 244-nm cw laser. Typical deviations are 15-20%. This may be due to the incomplete treatment in the model of the bleaching of the 242-nm transition and of the activation of the hydrogen. A more complete treatment of the bleaching could also further improve the agreement for the red luminescence curve.

Finally, during the work on the model we tried to make some predictions for new results. One of the first examples was some data for UV writing in fibres loaded with ultra-high pressures of hydrogen. At the time when we made the simulation we had no access to the detailed experimental parameters. We just tried to see if some realistic parameters could fit the data. The model result is shown in Fig. 4. We could only get satisfactory agreement with the data by assuming that the experiments were performed at very high UV-intensity ( $350\text{mJ}/\text{cm}^2$ ). With this value the agreement with the experimental results [29,30] is good. Later the actual experimental values were published, and we were very happy to see that the experimentalists had actually used this high pulse energy.

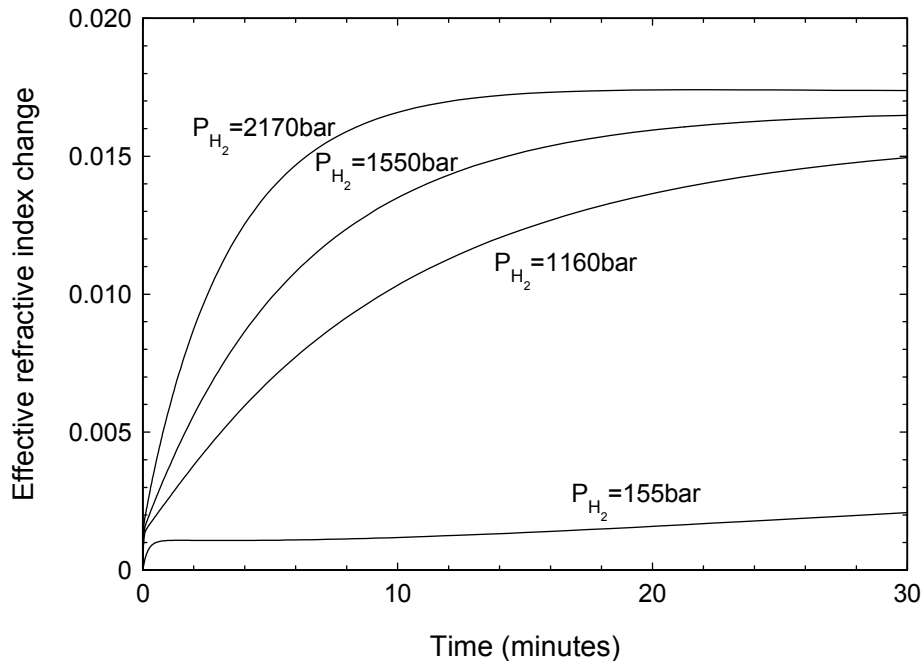


Fig. 4. Model predictions for writing in ultra-high pressure loaded fibre. The experimental parameters are 9 mole % Ge,  $\lambda=248\text{nm}$ , 50Hz repetition rate,  $I_{laser}=350\text{mJ/cm}^2$ . The curves are predictions of the average effective index change as a function of time for different loading pressures [28].

### ***Discussion and conclusion***

The dipole-quadrupole model for UV-induced processes in germanium-doped silica glass has been presented. The model is intrinsically of microscopic nature, but it should be emphasised that this does not rule out that part of the effect can be a compaction of the glass, since defects may well work to increase the density. However, one observation speaks partly against uniform compaction as the only dominant contribution to the effect. The UV-induced dispersion predicted by the model is in good agreement with results measured by a group in Moscow [31]. Pure compaction would lead to a different shape of the dispersion function in the visible part of the spectrum. Unfortunately the precision of the experimental results is insufficient to deduce the percentage of compaction and the percentage of deep UV absorption increase. Therefore we would recommend careful and very accurate measurements of the UV induced dispersion as a route towards better understanding of the fundamental UV-induced processes in silica glass.

The model assumes that germanium atoms work as gates for transferring energy into the material. By making plausible assumptions about the transfer mechanisms it has been possible to give a quantitative description of a very large number of experiments concerning UV-exposure of glass.

The model also assumes that two types of defects are formed. The absolute energies, thermal activation energies and rates for both these defects are determined. Their contributions to the index change are estimated. Generally, good agreement is found with experimental data, thereby justifying the basic assumptions of the model. It is able to describe results of UV-exposures using wavelengths within the range of the

242-nm absorption, at least one order of magnitude variation of the germanium concentration, most experimentally accessible hydrogen or deuterium concentrations and more than ten orders of magnitude variation in the UV-intensity. Furthermore, it describes the refractive index change including the properties of UV-written gratings, the change in absorption and the UV-induced visible luminescence.

Finally, it gives a good description of accelerated ageing experiments and normal thermal decay, and it is therefore able to predict the long-time stability of UV-written gratings. For this purpose one can use the following simple expression for the constants:

$$\begin{aligned}
 c_1 &= c_3 = 0 \\
 c_2 &= k_x \left( \frac{r_1}{r} \right)^{10} \exp\left( -\frac{\Delta E_x}{RT} \right) \\
 c_4 &= k_y \left( \frac{r_1}{r} \right)^{10} \exp\left( -\frac{\Delta E_y}{RT} \right)
 \end{aligned}
 \tag{3}$$

The most significant achievement is that the model uses one universal parameter set to describe all the results in a self-consistent way. Another important result is that it can explain the complicated structure of the red luminescence spectra and relate this to the fundamental structure of the glass determined from X-ray spectroscopy. Finally, it gives a more reasonable explanation for the thermal decay of UV-induced defects compared to previously presented models. Instead of assuming an unreasonably broad spectrum for the thermal activation energies it relates the behaviour to the radial dependence of the transition probabilities and the existence of two competing defects with opposite influence on the refractive index. It should be noted that this leads to the prediction that gratings written under different conditions such as UV-intensity, writing time, loading pressure and germanium concentration may have different stability and even qualitatively different decay curves. The model is able to make several new predictions of both detailed UV-writing experiments and of qualitatively new effects.

In conclusion, the UV dipole-quadrupole model presented here is a very useful tool for both physicists and chemists studying UV-induced processes and for engineers who would like to predict the performance of a new type of fibre or waveguide. The free parameters in the model have been determined by simple adaptation (without curve fitting) to a few spectra covering a large parameter range.

The most severe argument against the model is that it contains many free parameters. This is typical for a detailed description of a complicated amorphous material such as glass. The many parameters are also to a very large degree resulting from the need to describe many different types of effects, each demanding a few parameters (e.g. for normalisation). Of course it would be preferable if most of the free parameters could be determined from first principles. At the moment this is not possible, but for several

of the parameters such as branching ratios, absolute energy levels and the activation energies, there is good reason to expect that they can be determined from quantum chemical calculations in the future.

Finally, we would like to give a small word of warning. There are actually UV-induced effects in germanium-doped silica not described by the model. Here we do not think of the conceptually simple exceptions where the glass is doped with other materials than germanium and hydrogen. It is probably no surprise that this may lead to deviations. However, more subtle exceptions exist. Recently we found one of these [32]. It concerns UV-induced birefringence. Throughout the model description we have only considered average values of the UV-induced index change across the fibre or waveguide core. UV-induced birefringence probes exclusively the anisotropy. In this case we found that the dominant contributions come from interface defects and macroscopic stress due to the presence of hydrogen. However, the absolute size of these effects is typically 30 times smaller than the average UV-induced effects.

### ***Phenomenology of grating writing – practical aspects***

The theory describing the effects of UV-induced index changes in connection with technologically simple gratings in fibres and waveguides has been presented above. Today commercial programs are available for simulations of Bragg gratings under the assumption that the index changes are linear. However, it may be appropriate to take a quick look at some of the limitations of standard grating theory in general and simulation programs in particular. These limitations fall in two categories. One type of limitation is primarily related to incomplete knowledge of the detailed effect of non-perfect phasemasks used together with imperfect laser beams, and in combination with non-linear UV-induced index changes. It is fair to say that this is not really a limitation for the simulation programs, but rather due to the limited knowledge possessed by the users. In most cases it is nearly impossible to measure the experimental UV-power and phase distribution in the near-field of a phasemask. The best alternative is making an independent characterisation of the phasemask and laser beam, and to do a vector diffraction analysis of the near field pattern. Since vector diffraction is cumbersome, this is never done in practice.

Another type of limitation, which is sometimes important, is that practically all theoretical treatments of Bragg gratings assume that the gratings make negligible perturbations to the waveguide confinement. For weak Bragg gratings in standard fibres and gratings up to intermediate strength in waveguides with higher core-cladding index steps (and far from the cut-off wavelength!) this is an excellent approximation. It is even so that the approximation belongs to the type of fortunate cases, where meaningful results come out well beyond its simple range of validity. However, it always breaks down when the maximum index change somewhere along the grating becomes so large that the core locally becomes multi-mode. Often the transition between the ‘perturbative’ and ‘non-perturbative’ regime is dramatic with several tens of dB change in the transmission and reflection spectra within a few tens or hundred pulses of UV-exposure in an otherwise 25000-pulse long grating exposure [33]. The extreme limit of non-perturbative behaviour occurs in photonic bandgap

(PBG) structures, which in many respects can be considered as extremely strong gratings in multiple dimensions.

Bragg gratings obtained by UV-writing with a 193-nm excimer laser, which has particularly poor beam quality, clearly illustrate some of the problems related to imperfect beam and phasemask quality together with non-linear index changes [34]. A very simple model for grating growth relates the Bragg grating strength in transmission to the average refractive index change in the core. Strictly speaking the model is only valid when the refractive index change is a spatially local, analytical function of the UV-fluence. This is normally the case when the visibility of the UV-pattern is low to moderate and the intensity is not too high. These approximations are normally fulfilled when using 193nm because of the poor beam quality and since it is not recommended to focus the beam too tightly due to risk of electric breakdown in air. However, when using a high-power beam with reasonable spatial coherence at 248nm the basic approximations may break down.

In brief, the simple phenomenological model [34] can be explained the following way. When a fibre or waveguide is exposed to a uniform UV-interference pattern, the local effective refractive index change,  $\Delta n$ , as a function of position,  $z$ , and UV-fluence,  $F$ , is given by

$$\Delta n(F, z) = \Delta n_{avg}(F) + \Delta n_{mod}(F) \sin(kz)$$

$$k = \frac{2\pi}{\Lambda}$$
(4)

where  $\Delta n_{avg}$  is the average effective index change, which can be calculated from the measured shift in Bragg wavelength,  $\Delta n_{mod}$  is the modulation amplitude for the grating and  $\Lambda$  is the grating period. Under the assumptions described above the modulation amplitude can be written

$$\Delta n_{mod}(F) = \frac{1}{2} |\Delta n((1 + \nu)F) - \Delta n((1 - \nu)F)|$$
(5)

where  $\nu$  is the grating visibility. Fig. 5 illustrates the quality of the model. The grating strength has been fitted using input from the average effective index change with  $\nu$  as the only free parameter. The best fit was found for  $\nu=0.07$ . The quality of the fit is good considering the experimental uncertainty. The value of  $\nu$  is close to what can be expected when using the specified beam quality of the laser together with the phasemask data in a Fresnel calculation of the diffraction pattern [34].

In conclusion, the simple phenomenological model shows good agreement with a series of experiments performed with different fibres using 193nm. In particular it explains the oscillations in grating strength as a function of exposure time using the observed variations in the average refractive index. As expected the simple model breaks down, when the fundamental assumptions are no longer valid (e.g. for high power or high visibility). However, it can still be used to give a crude qualitative

explanation of the shape of the curves for the grating strength. It is therefore a handy tool for the experimentalist, but not particularly useful for describing details of advanced gratings. Probably the main drawback is that it is necessary to measure the average refractive index curve before it can be applied. The reason is of course that the simple phenomenological grating writing model does not include any theory for the basic UV-induced index changes. This may be remedied by combining it with the advanced microscopic model described above.

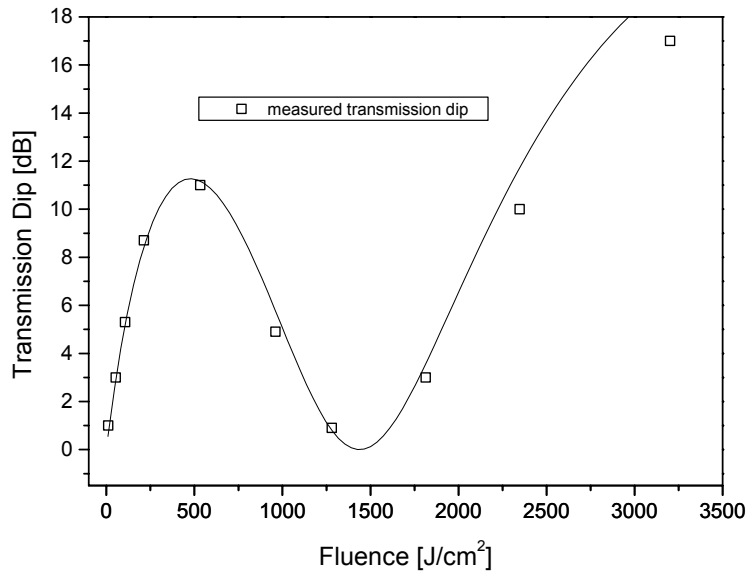


Fig. 5. The calculated grating strength based on the measured effective refractive index shift and the simple phenomenological grating writing model (solid curve) is in good agreement with the directly measured result (open squares) when the visibility,  $v$ , is used as a free parameter [34].

Another consequence of imperfect writing conditions is the formation of higher-order gratings in the fibre or waveguide. These are rarely observed since in most applications they have no influence on the results, and since users often do not care to look for them. However, such higher-order gratings are often surprisingly strong as illustrated in fig. 6. The primary reason is that the presence of just minute amounts of 0<sup>th</sup> order or +/-2<sup>nd</sup> order contributions in the UV-diffraction pattern from the phasemask gives rise to significant modulation strength at the same period as that of the phasemask [35,36] and at higher orders from this (half integer orders compared to the 'normal' grating). For the same reason one would also expect that it would give rise to a 0.5 order (sub-harmonic) grating, but since this typically lies around 3.1  $\mu\text{m}$  in wavelength this is never observed.

Even in case one has an ideal phasemask there will still be some grating strength at higher integer orders. This is due to the non-linear UV-induced index change as a function of the fluence (and for pulsed lasers also as a function of the intensity).

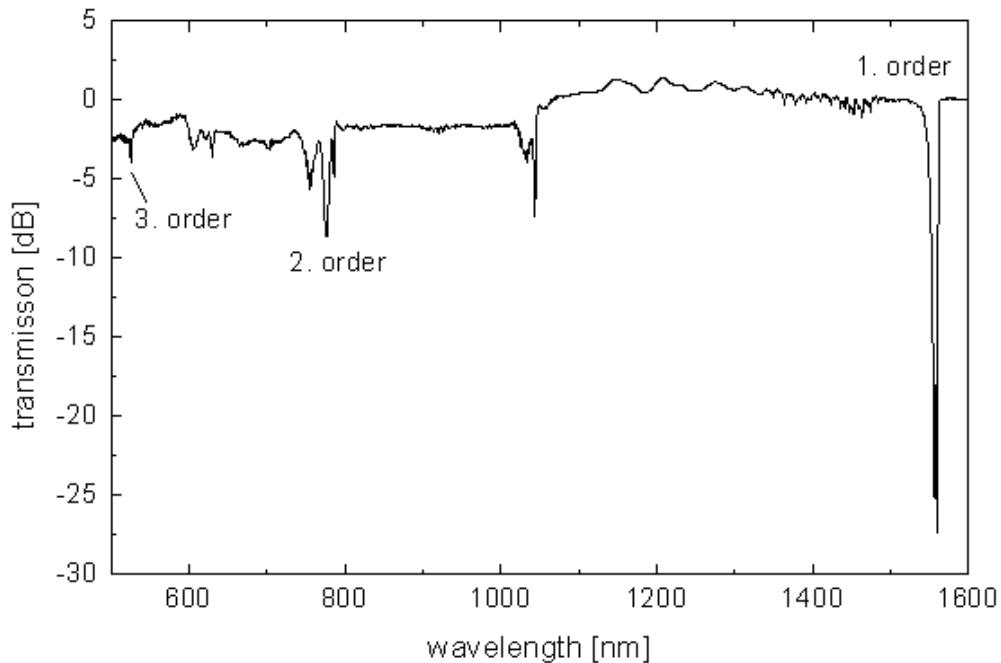


Fig. 6. Observation of higher-order gratings due to the influence of a non-linear UV-induced index change as a function of fluence in combination with diffraction orders different from  $\pm 1^{\text{st}}$  from the phasemask [33]. The non-integer grating orders observed near 625nm and 1050nm are only possible due to interference between the  $\pm 1^{\text{st}}$  orders, and either  $0^{\text{th}}$  or  $\pm 2^{\text{nd}}$  order contributions in the phasemask diffraction pattern [35]. The integer grating orders can be observed even for a perfect phasemask (with no  $0^{\text{th}}$  order or  $\pm 2^{\text{nd}}$  order diffraction) if the UV-induced index change is non-linear.

## Fabrication methods for fibre Bragg gratings

Excellent reviews on the fabrication methods and experimental results obtained with fibre Bragg have been written by Kashyap [22] and Othonos [37]. For readers who are new to the field we highly recommend consulting these sources of information. In the following we will give a focused and specific, but much less comprehensive list of selected methods and examples.

### *Phase mask dither method*

One way to realise a flexible writing method for advanced gratings using only one exposure has been demonstrated by University of Southampton and a few other groups across the world [38]. In brief, their method uses controlled dithering of the phasemask or the fibre in order to control the local grating visibility and phase. This method allows writing of very long gratings of extremely high quality [39], and it is today the preferred method for fabrication of the most critical gratings, such as those used for dispersion compensation [40].

A selection of impressive results obtained using this method has been presented in a large number of invited talks at major conferences, in particular by Morten Ibsen. Unfortunately very few of the intimate technological details have been published. Simplified setups for realising the method are today commercially available.

However, the method is technologically difficult to implement in an optimum way since it demands extreme interferometric stability of the entire set-up. The equipment is also rather expensive and the throughput per production line is modest when a high grating quality is needed, which may pose a problem for high-volume production. Therefore there has been considerable motivation for the development of alternative methods for writing advanced Bragg gratings.

### *Polarisation-control method*

The polarisation-control method for Bragg grating writing relies on changing the polarisation of the UV-beam during exposure [41-44]. It requires only a single scan at constant speed. The principle of the method is illustrated in Fig. 7. A polarisation beam-splitter is scanning along the phasemask together with the UV-beam. Two spatially separated Bragg gratings are generated in the waveguide by the diverging *s*- and *p*-polarised fractions of the UV-beam. A high-power polariser mounted in a rotation-stage controls the polarisation of the UV-beam from the excimer laser. The small remaining elliptical polarisation in the primary laser beam was compensated before passing the polariser by an uncoated silica window, which was rotated until the laser polarisation became uniform. The polariser's angle with respect to the *s*-polarisation is denoted  $\alpha$ . The total UV-fluence after the polariser is  $F$  and the fluence in the *s*- and *p*-polarisations are  $F_s = F \cos^2 \alpha$  and  $F_p = F \sin^2 \alpha$  respectively. The average

fluence is always constant since  $\cos^2\alpha + \sin^2\alpha = 1$ . By choosing the proper distance between phasemask and waveguide core (i.e. phase-shift between parts of the grating induced by *s*- and *p*-polarised light) and polarisation angle,  $\alpha$ , any type of grating can be fabricated. In particular, if the distance is chosen in such a way that the phase-shift between the two gratings is equal to  $\pi$ , the modulation will be proportional to  $\cos^2\alpha - \sin^2\alpha$ , which can assume any value between  $-1$  and  $1$ . A simple formula is given [42,43] for calculating the optimum distance,  $d_{air}$ , between the fibre and the phasemask in order to obtain a phase-shift of  $\pi$ :

$$d_{air} \approx \frac{\Lambda_{mask}}{4\theta} - \frac{r_{fibre}}{n_{clad}} \tag{6}$$

Here  $r_{fibre}$  is the fibre radius,  $n_{clad}$  is the refractive index at 248nm of the fibre cladding,  $\Lambda_{mask}$  is the period of the phasemask and the divergence angle,  $\theta$ , between the two polarised beams is assumed to be so small that  $\tan\theta \approx \sin\theta \approx \theta$ . With this setting it is possible to make any (real-valued) apodisation profile. More exotic types of apodisation or phase-shifts can be realised by choosing a different distance to the phasemask. However, it is important that the distance from the polarisation beam splitter to the fibre is kept so short that the two beams from the beam-splitter do not separate spatially to any significant extent. Furthermore, the polarisation beam splitter angle should be chosen so  $d_{air} > 0$  and the total distance from the phasemask to the core is significantly smaller than the spatial coherence length of the laser.

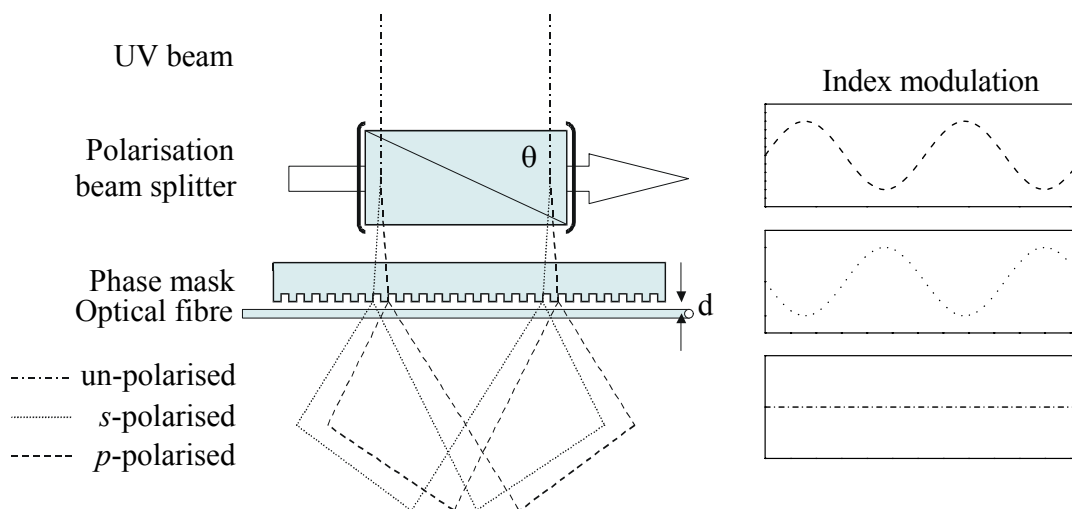


Fig. 7. Illustration of the polarisation-control method for Bragg grating writing. A polarisation beam-splitter discriminates between the *s*- and *p*-polarised fractions of the UV-beam. Selecting the proper distance between the phasemask and the fibre generates two independent Bragg gratings with a controlled phase difference. Hereby any kind of apodisation including fixed phase-shifts becomes possible [43].

For the initial experiments we used a Wollaston prism polarisation beam-splitter with a  $0.15^\circ$  divergence angle and a  $125\text{-}\mu\text{m}$  diameter fibre, which makes  $d_{air} \approx 60\mu\text{m}$  the

optimum distance for  $\pi$  phase-shift for a Bragg grating around 1550nm. However, in order to obtain perfect performance it is necessary to correct for the fact that  $\theta$  is not infinitely small and the optimum distance then becomes a few  $\mu\text{m}$  larger [45].

Until now the new writing method has been used to fabricate Bragg gratings with a phase-shift and Bragg gratings apodised with a Gaussian function and/or a sinc function. The first two types of Bragg gratings look quite similar to what can be made with a conventional double exposure. An example is shown in Fig. 8. It is compared to results from theoretical simulations using the commercial software IFO gratings [46]. Sinc apodised Bragg gratings cannot readily be made with the simple double exposure method. In principle they should be significantly better than Gaussian apodised gratings (which can be made by double exposure) in the case of weak gratings because of the Fourier-transform relation between the box and sinc function. In Fig. 9 experimental results for a strong sinc grating are compared to theoretical simulations performed using the IFO grating program. For strong gratings it is necessary to modify the profiles, so they only remain 'sinc-like'. This way it is also possible to design gratings, which have reduced dispersion in reflection from one end [47,48]. This property is very important for some system applications in particular when using very high bit rates per channel [49,50]. Below we describe results obtained with optimised sinc-like gratings written using the polarisation-control method. The experiments indicate that this combination is very successful [51], and in particular for very strong gratings it is most likely better than the phasemask dither method. For weak gratings the phasemask dither method is clearly superior.

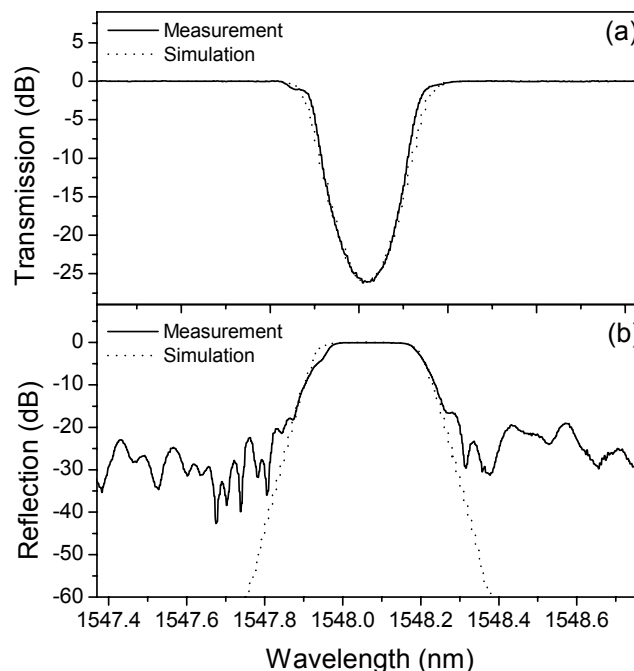


Fig. 8. Transmission (a) and reflection (b) spectra for a 23mm long Gaussian grating written in a deuterium-loaded TrueWave<sup>®</sup> fibre with the polarisation control method and compared to theoretical simulations using IFO-gratings [42,46]. The high background reflection level far from the grating centre is due to spurious reflections during the characterisation (from a poor splicing).

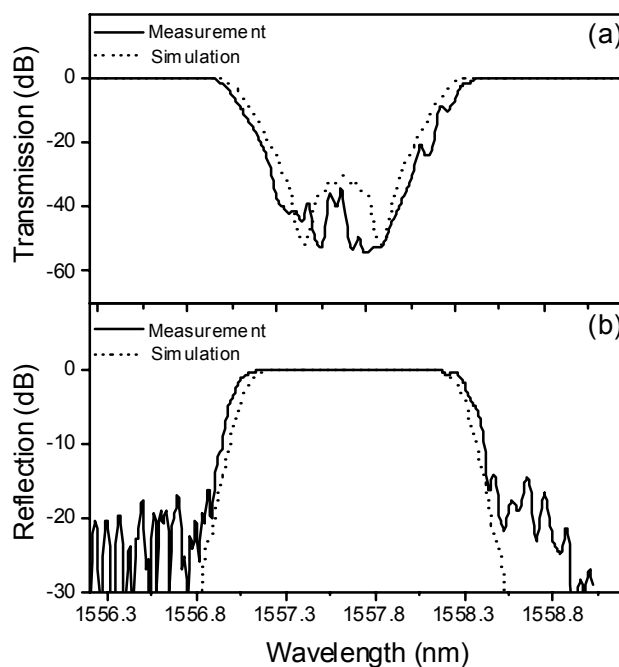


Fig. 9. Transmission (a) and reflection (b) spectra for a 23-mm long sinc grating written in a deuterium-loaded highly non-linear fibre (HNLF) [42].

In some cases the effective photosensitivity of the medium may be slightly anisotropic. In such cases the refractive index changes induced using *s*- and *p*-polarisation are different and the grating becomes birefringent [41]. Normally this effect is highly undesired, since it will lead to polarisation dependent loss (PDL), polarisation mode dispersion (PMD) and non-ideal filter functions for the grating-based components. Naively one would expect that such effects would be exacerbated by the polarisation-control method. However, experimental investigations have shown that in all known cases where the effect is observed, it can easily be removed with a very weak post-exposure (typically with 100 times less fluence than used during the writing) with UV-polarisation parallel to the core [41,42].

In case it is the intention to write gratings with special polarising properties the anisotropy may even be an advantage. In this case the new writing method can in principle be used to write gratings that perform conversion from TE to TM and gratings, which reflect preferably one of the polarisations [41]. Such gratings have not yet been fabricated, but it is believed that the new method will be superior for this purpose compared to all other methods, since it has built-in polarisation control. It should also be mentioned that this application is not limited to Bragg gratings, but may be used in many other cases, e.g. for the fabrication of long-period gratings.

Finally, it is worth considering that there may be other types of advantages of the polarisation-control writing method. These include the possibility to write blazed gratings with controlled coupling to cladding modes by using a beam-splitter with a much larger separation angle. It is also possible to control the strength of higher order reflection gratings by using magic phase-shifts, typically obtained with very small separation angles. Yet another possibility is to reduce the influence from reflections from e.g. silicon substrates below buried waveguides by choosing the geometry in

such a way that the interference pattern from the reflections cancel out. The same trick may also be applied to write gratings selectively in one layer of a chip with multiple layers of waveguides. These advanced applications are described in detail in the patent application for the polarisation-control method [41].

In conclusion, there is still much work to do before the polarisation-controlled writing method becomes fully commercial. In particular there are two outstanding issues. One problem is the non-linear dependence of the refractive index change on the intensity and fluence of the UV-light. In cases where the advanced microscopic model described above agrees well with the data this problem can formally be solved by using output from the model as input for a grating simulation program. However, what is really needed is the inverse operation. This can be obtained either by solving a very complicated inverse scattering problem [52] or, if the writing can be parameterised in a moderate number of slots, by using a least squares fitting procedure, e.g. Marquardt's method [53]. Both methods are rather cumbersome to implement, and will demand significant CPU processing time. The other problem is the experimental optimisation of the writing. Until recently the main source of experimental error was that the first polariser moved the beam when it was rotated. Replacing the polariser with one, which did not have a wedge-like shape, solved this issue and improved the experimental results significantly. After implementing this and performing many other small improvements the grating quality is now clearly superior to that obtained with conventional double exposure methods. It is therefore fair to conclude that the method is possible to implement in a production environment.

## Grating applications

### *Simple filters*

The electromagnetic theory describing the effects of simple gratings in fibres and waveguides is well-described in several references [22,37]. This white paper will instead focus on a few selected examples of interesting and advanced grating types.

### *Advanced filters*

Apodisation profiles for advanced filters can be designed using various methods including genetic algorithms [54], inverse scattering [52], inverse scattering in combination with some iterative tricks [55] and gradient-based methods [56]. Today the most commonly used methods in commercial applications are those based on inverse scattering in combinations with selected tricks. However, according to our experience the gradient-based methods are the most effective. One example of a design is shown in Fig. 10. The superiority of gradient-based methods becomes even more obvious for gratings in multiple dimensions, where the closely related topology-optimization method delivers superior results for planar PBG components [57].

The advanced filter gratings can be fabricated with any of the methods described in the paragraph on fabrication methods. Below we have used results obtained with the polarisation-control method [42] as examples. However, in general the phase-mask dither method provides the highest flexibility and the highest quality gratings with the exception of very strong gratings. In this case the polarization-control method is superior.

Fig. 11 shows transmission, reflection and phase delay spectra for the advanced grating from Fig. 10 fabricated with the polarization-control method [58]. The design was optimised in such a way that the bandwidth utilisation for 10Gbit/s signals was maximised. This was obtained by simultaneous minimisation of the dispersion, flattening of the peak of the reflection spectrum, optimisation of the steepness of the flanks while simultaneously keeping a minimum grating strength.

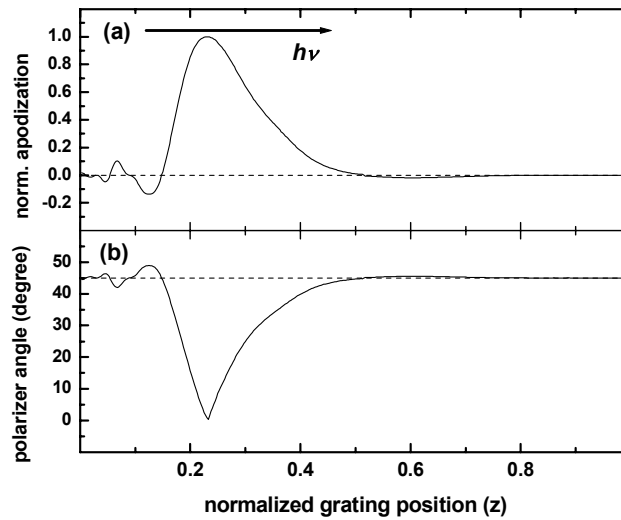


Fig. 10. (a) Designed apodisation profile (negative values indicate a  $\pi$  phase shift) for a grating designed to have maximum bandwidth utilization at 10Gbit/s. The design is optimised by the method described by Plougmann and Kristensen [56]. (b) Calculated polarizer angle for fabrication of the grating using the polarization-control method.

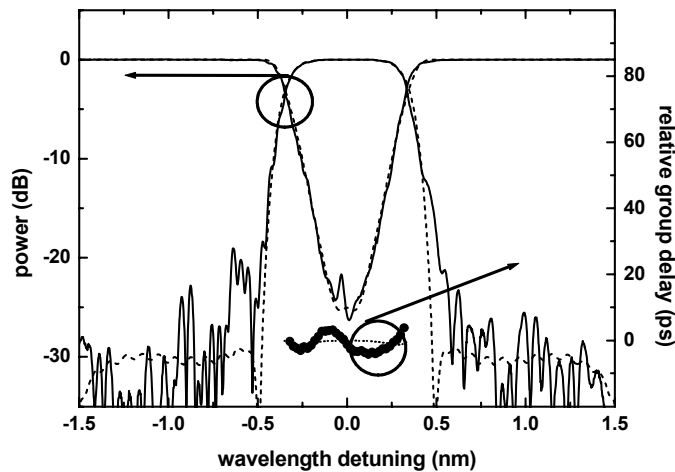


Fig. 11. Transmission, reflection and dispersion spectra for the filter optimised for maximum bandwidth utilization with 10Gbit/s signals [58].

Fig. 12 shows results from transmission experiments using the grating as a filter. If the bandwidth utilisation is defined as the region with less than 1dB penalty (many other definitions are possible, but the technical details lie far beyond the scope of this text), then the bandwidth utilisation is close to 100%, e.g. the entire bandwidth of the grating can be used for transmission!

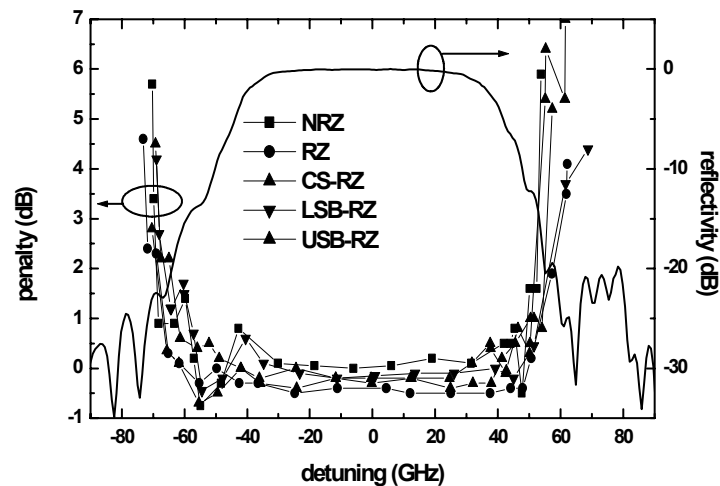


Fig. 12. Transmission penalty as a function of detuning for different modulation formats transmitted through the bandwidth utilization optimised grating together with the reflection spectrum. The grating has close to 100% bandwidth utilization at 10Gbit/s [59].

### *Add drop multiplexers*

As the fabrication process for waveguides matured and the design possibilities improved it became possible to fabricate high-quality OADM-devices (Optical Add Drop Multiplexers) for system applications from around 1995 [60-62]. Initially the multiplexers were using simple grating filters, but gradually more advanced gratings have been applied.

OADM-devices are key components of WDM networks. Several techniques and designs may be used in order to achieve this functionality in integrated optics [63-66]. Bragg-grating-based devices are of great interest since they enable construction of compact devices with transfer functions, which can easily be altered by changing the grating parameters. When the Bragg gratings are written in the arms of a planar Mach-Zehnder interferometer, they realise an OADM with potentially low crosstalk. Moreover, the device drops one channel without altering the others, thus enabling cascading of several devices and flexible use in systems with an ever-increasing number of channels. However, it is difficult to make the device tuneable due to the low thermo-optic coefficient of silica and high Young's modulus for both silicon and silica. This is a significant disadvantage for system applications.

As an example, the EU-METON OADM-devices were fabricated in the following way: The waveguides had Ge-doped cores with index step to the cladding of  $7 \times 10^{-3}$  and core dimensions of  $6 \times 6 \mu\text{m}^2$ . The structure of the multiplexer is shown in Fig. 13. It is composed of a 51mm long Mach-Zehnder interferometer with identical 3dB directional couplers. The Bragg gratings were simultaneously induced in the two arms of the interferometer by illuminating the waveguides with UV-light at 248nm through

a phasemask. Prior to the grating fabrication, loading with ~2mol% deuterium was used to enhance the photosensitivity.

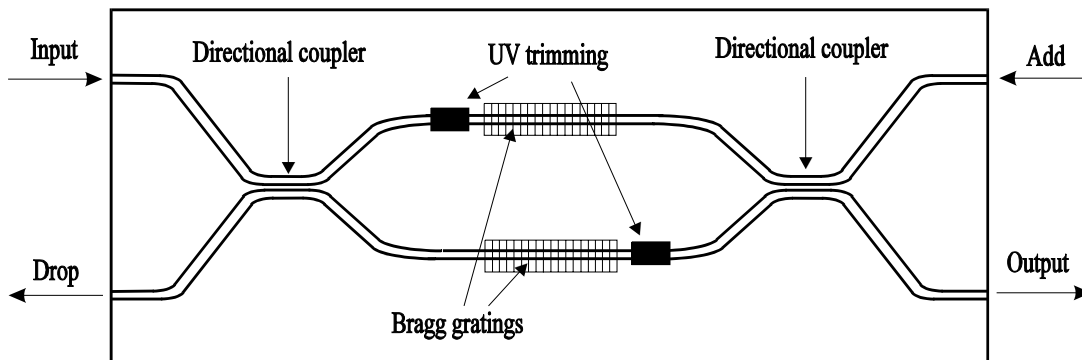


Fig. 13. Layout of the grating-based integrated OADM device [62].

Deuterium is preferred compared to hydrogen for fabrication of commercial devices since its use gives rise to much less absorption in the glass than hydrogen does. This has two reasons. First of all some of the intense overtone bands of OH, NH, SiH and GeH lie only slightly below 1550nm. Use of deuterium gives rise to a shift in the vibrational wavelengths of  $\sim\sqrt{2}$ , whereby they shift to around 2000nm, which is well outside the wavelength range used for telecommunications. An added advantage is that since the vibrational levels lie closer to the bottom of the electronic potential curves, the parabolic approximation for the potentials is better. Therefore, the Franck-Condon factors, which are equal to zero in the case of a perfect harmonic oscillator with a pure parabolic potential, are very small for the deuterated compounds. This gives rise to a general reduction in the transition strength of all overtone transitions by more than one order of magnitude.

The beam from the excimer laser was uniform in one dimension and approximately Gaussian in the other dimension. The Gaussian shape was used for apodising the gratings. The  $1/e^2$  diameter of the beam was 11mm and the total fluence used for the exposure was  $3.7\text{kJ}/\text{cm}^2$ . After exposure the wafer was heated to  $80^\circ\text{C}$  for 10 hours to remove the unstable index-changing defects and remaining deuterium.

The device was characterised by an ASE source near 1550nm and an optical spectrum analyser. Two fibres in silicon V-grooves were butted up to input and output ends of the multiplexer to allow measurements of the power transmitted to all ports. The input fibre was also connected to a three-port circulator in order to record the back-reflected signal. The spectra were then normalised to the output spectrum from the ASE source measured directly from input fibre to output fibre. Fig. 14 shows the transmission from the input to the output port and the signal reflected to the drop port. For the 400GHz ( $3.25\text{nm}$  @ 1559nm) channel spacing, which the device was designed for, the isolation of the adjacent channel is better than 27dB. The transmission dip is stronger than 50dB. Its strength determines the isolation between the drop and add channels, the so-called intra-band crosstalk.

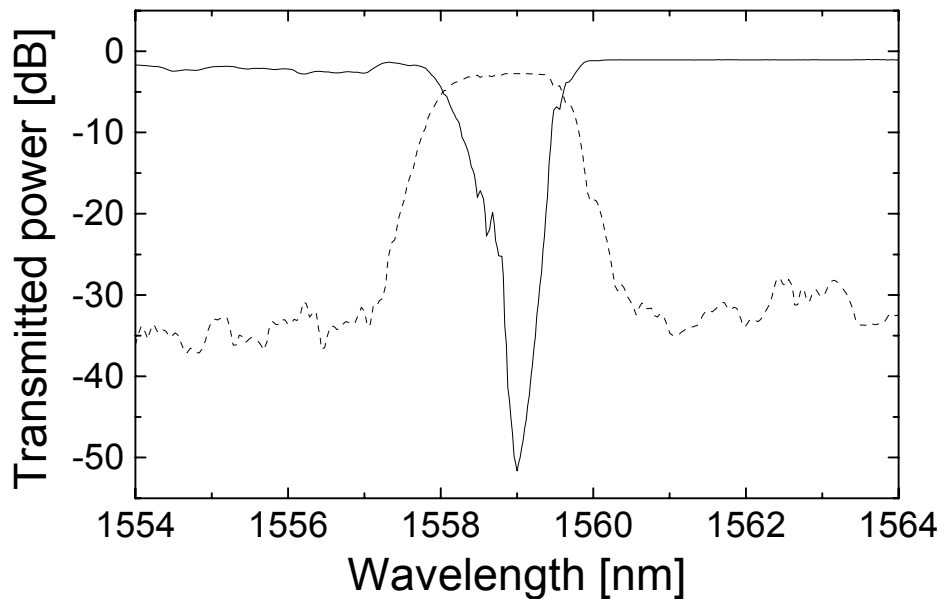


Fig. 14. Transmission and reflection spectra from the grating-based OADM device [62].

The insertion losses in transmission are 1.0dB for wavelengths longer than the Bragg wavelength. On the short wavelength side, some residual coupling to the cladding slightly increases this value to ~2dB. At the drop port the losses at the Bragg wavelength are also ~2dB. This is mainly due to misalignment of the fibre pair, and was slightly improved when the device was permanently fibre pigtailed.

In conclusion, the device fulfilled the specifications set out by the project and performed well in the system tests. To the best of the author's knowledge it still possesses the best specifications for integrated, grating-based OADM devices. However, it has not yet gone into production. Presumably part of the reason is that it is not tuneable. In addition there is stiff competition from arrayed-waveguide-grating (AWG) based devices. These can be produced exclusively using clean-room processes, and they are therefore less labour-intensive to mass fabricate, which takes supremacy over the higher initial costs and larger consumption of silicon real estate.

The next subject to mention within the waveguide-based devices is the use of UV-light for tuning clean-room-fabricated devices. Work on this subject was also initiated under the METON project for two independent reasons. First of all it was believed initially that it would not be possible to place the Bragg gratings in the Mach-Zehnder interferometers with sufficient precision to ensure that the reflection came out of the drop port and not partially back into the input. In the end this was, however, done successfully, and the remaining reflection was kept below -17dB at the very worst wavelength (specifications were rather modest: -15dB). Therefore, OADM trimming did not become necessary. The other reason for UV-trimming was that there was some risk that the AWG's produced for the project could not hit the proper wavelength. Also in this case the reality came to be better than expectations, so

trimming was not needed in the end. However, since AWG UV-trimming had never been done before we decided to try it on a spare device. The result was successful [67], but since deuterium loading [68] was needed, it was not easy to hit the target wavelength precisely.

### ***DFB fibre lasers***

Fibre lasers have been important research subjects for several groups during the past 15-20 years. A very large number of different lasers have been developed but only some of these have since then attracted commercial interest. UV-written fibre DFB lasers were invented in competition between a few groups across the world [69-73]. Our initial contribution to the field was to demonstrate the first completely UV-written erbium-doped DFB laser, which was robustly single-mode [73]. In addition we have demonstrated high-quality multi-wavelength sources [74], very stable single-mode and narrow-band operation [75], operation up to 1618nm [76], and proven the connection between a birefringent phase-shift and single-mode operation [77,78]. Finally, the technology was successfully transferred to Koheras, where the inventions are today used commercially.

Single-frequency lasers emitting around 1550nm are important parts of optical communication systems today. Until the early nineties only semiconductor technology was capable of providing lasers of sufficient quality and acceptable price for this purpose. The different types of semiconductor laser types consist of DFB and DBR lasers, which are compact, normally fibre-pigtailed sources. In addition there are external cavity lasers, which are bulk devices consisting of a laser chip and a motor-controlled classical grating. They have great flexibility, particularly tunability, but rather high price. The fibre DFB lasers have shorter tuning range, but their main advantages are the great stability, the compact packaging, the good noise properties and the narrow linewidth. These properties are quite good for telecommunication applications but excellent for sensor applications. An added advantage for sensor applications is that a short tuning is simple and relatively inexpensive to perform.

For researchers with a background in semiconductor lasers the name fibre DFB laser may sound a little confusing because the realisation of distributed feedback in many modern semiconductor lasers is somewhat different from the case of fibre cavities. In the fibre and glass waveguide case the DFB cavity consists of a long grating with one (or possibly several) distributed phase-shift(s) near the middle. The DBR (distributed Bragg reflector) fibre laser, on the other hand, is characterised by having short Bragg gratings in each end of a grating-free cavity.

For the first demonstration of UV-written fibre DFB lasers we used an Er-,Al-,Ge-doped silica based fibre with an erbium concentration of  $1.5 \times 10^{25} \text{m}^{-3}$ , a numerical aperture (NA) of 0.27 and a core diameter of 4 $\mu\text{m}$  fabricated by Lucent Denmark (now OFS Fitel Denmark). This fibre has a combination of good properties for the laser performance, particularly the germanium-doped ring around the core, which facilitates writing of birefringent phase-shifts allowing single-polarisation behaviour

[78]. Later, single-mode DFB fibre lasers were also realised in a number of other fibres [76,79].

In brief, DFB fibre lasers are fabricated as follows. At first it is necessary to choose an appropriate rare-earth-doped active fibre (typically doped with erbium and/or ytterbium) with sufficient UV-sensitivity to enable writing of strong Bragg gratings. Both ends of the active fibre are spliced to standard fibre (e.g. SMF28 or corresponding Lucent fibre). Some improvement of the output power can be obtained by inserting a fibre with properties intermediate between the standard fibre and the rare-earth-doped fibre because it helps to bridge the significant differences in core size. If the ultimate performance in terms of suppression of amplified stimulated emission (ASE) noise is desired, it is also important that the length of the active fibre is only slightly longer than the grating. The reason is that any part of the active fibre outside the DFB cavity will emit ASE and raise the noise floor. On the other hand, it is sometimes more important to increase the output power than to achieve the ultimate suppression of the noise floor. In such cases it is possible to insert some additional length of active fibre and use the remaining pump power for amplification in a master oscillator power amplifier (MOPA) configuration [74]. The output of such an amplified DFB fibre laser is shown as the insert in Fig. 15.

After splicing the fibres together the long cavity-forming grating must be written. It is most usual to use a uniform grating, but in special cases it may be better to use some kind of apodisation to suppress additional kinks in the grating transmission curve. For DFB lasers near the maximum of the erbium gain curve (from 1528nm to 1570nm) the exact grating strength is not critical for obtaining single-mode lasing. However, cavities with very weak gratings will not oscillate or only do so at exceedingly high pump powers. Too strong Bragg gratings may show laser action even without phase-shifts and will often give rise to longitudinally multi-mode lasers, particularly if there is some chirp in the grating.

Finally, the phase-shift must be induced. It is typically done by replacing the phasemask with a few mm long opening and continuing UV-exposure in that region. This is the most critical part of the fabrication since the phase-shift must be very accurate in order for the laser to work properly. For effectively discrete phaseshifts in long, weak gratings the phase-shift must be  $\pi$  [77] ( $\pi/2$  in terms of the optical wave [73]). There are a couple of reasons that the phase-shift is delicate to make. First of all the refractive index shift induced by the UV-light initially assumes a value slightly higher than the stable value and simultaneously the UV-light induces some colour centres, which give rise to loss. Most of the non-permanent index increase and loss decay within a few minutes at room temperature. However, if the DFB laser needs to be stable for many years, it is necessary to anneal it at 100°C or higher for some hours in order to remove more of the unstable UV-induced defects. Parasitic processes driven by the UV-light probably induce the very short-lived defects and colour centres. However, the model in chapter 4 describes the defects that need to be removed by annealing at 100°C, at least in germanium-doped silica. Because of these phenomena it takes significant experience to induce the correct phase-shift in an unknown grating. Alternatively one can work very slowly based on trial and error and induce some phase-shift, allow approximately 10 minutes for the most unstable

defects to decay, characterise the laser, induce additional phase-shift, and continue until the laser is good. Then one additional step should be taken past the optimum before the laser is removed from the set-up and annealed bringing it back to optimum, but this time with a stable performance.

Another reason that the phase-shift is delicate to make is that its birefringence controls whether the laser becomes polarisation single-mode or double-mode [78]. This has been predicted theoretically and tested very carefully in experiments by gradually increasing the phase-shift and monitoring the power in the two polarisation modes [77]. Fibres with a UV-sensitive ring around the core are particularly good for inducing a stable birefringent phase-shift of correct magnitude, and this is indeed one of the most important reasons that our first choice of fibre was excellent. Many of the details are described in a patent [78], and since some of the rest is still considered commercially sensitive, no more details will be given here.

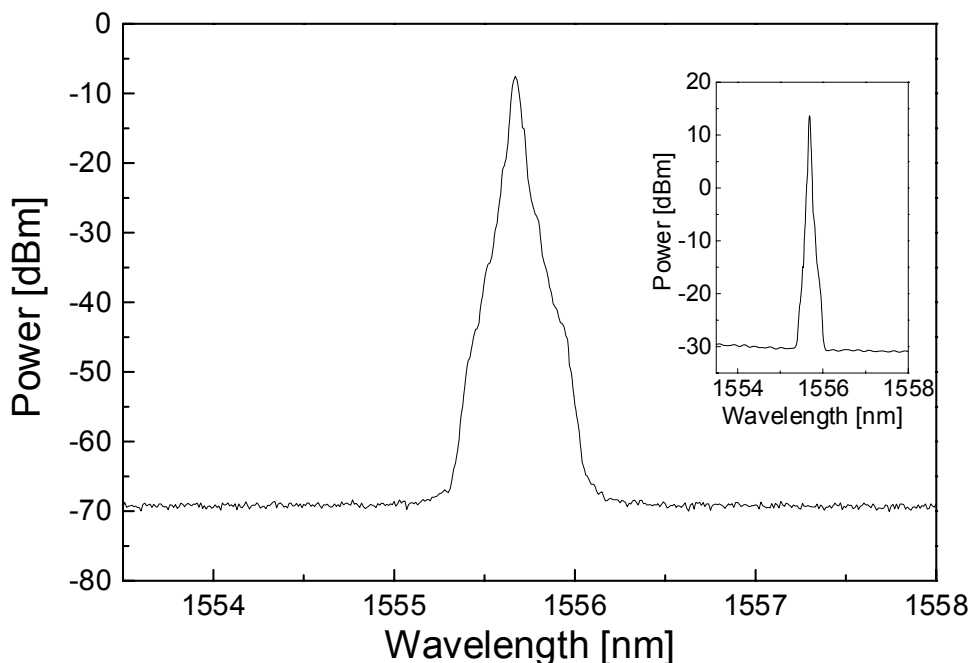


Fig. 15. DFB fibre laser measured with an optical spectrum analyser (OSA). The shape is the OSA filter function. Insert: Output after amplification in a MOPA using the remaining pump power [74].

The properties of the DFB fibre lasers have gradually improved as more information was gathered through the research. During the commercialisation process further improvements have also been obtained; - particularly within the areas of fibre handling, output power increase, reproducible fabrication and packaging. The final development-related improvements have largely been obtained without contributions from the author and, besides, they are all considered trade secrets. Therefore no further description is given here. However, some of the improvements obtained through research at COM are quite interesting. A few examples are described below.

Initially the output power of the erbium-doped DFB fibre lasers was only around 20 $\mu$ W for 50mW pumping at 1480nm [73]. There were several reasons for this low

power. First of all the early lasers were written with 193-nm UV-light [73]. Irradiation with photons of so short wavelength induces some additional loss in the glass compared to UV-writing with e.g. 248nm. The reason is probably different types of radiation damage processes. Optical loss inside a laser cavity is extremely severe for the output power since the photons travel several times through the lossy area. After switching the writing wavelength to 248nm, typical output powers increased to 150 $\mu$ W. Additional small improvements were obtained by pumping at 980nm rather than 1480nm, by increasing the pumping power, by more carefully designing the grating strength [75,76], and by increasing the cavity length. However, more than 1mW output power could only be obtained in our research set-up by using co-doping with ytterbium in order to increase the pump absorption.

All the physical changes that increased the output power (with some reservation concerning ytterbium co-doping) also increased the signal to ASE ratio, improved the laser stability, decreased the relative intensity noise (RIN) and decreased the laser linewidth. As examples the first lasers had typical signal to ASE ratios of 35dB, while some of the later ones had more than 70dB, initially linewidths were around or slightly below 15kHz; - later 1kHz was reached. When discussing the signal to ASE ratio it is relevant to mention that the side-mode suppression is significantly better than this number. In fact the side-modes were practically always so weak that they could not be observed in the ASE background.

As the lasers improved we made different test experiments with them. One very popular type of test was to use DFB lasers as sources in bit error rate experiments. In all cases they compared favourably with semiconductor lasers. The only disadvantage is that their linewidths are in some cases smaller than desired, since even reflections from 50km distance are completely coherent, which most system and network experts dislike because of the properties of typical networks today.

Temperature cycling is another popular type of test. Some of the lasers have remained single-mode when cycled down to 77K and all the way up to 600K. Above 600K the lasers generally have short lifetimes, but they sometimes remain single-mode until they stop lasing! The high temperature behaviour can probably be improved since according to the predictions of the dipole-quadrupole model it is possible to increase the stability of the gratings by inscribing them with higher UV-fluence and removing the excess strength by annealing. At 77K the performance of a laser operating near the gain peak of erbium is improved resulting in higher output power and lower laser threshold than at room temperature [33]. When cooling further to 4K some new phenomena are observed. First of all there is a tendency that the laser threshold becomes very low and less sharp. However, simultaneously some of the lasers show longitudinal multi-mode operation. In addition, interpretation of the results becomes difficult because of insufficient fundamental data, particularly on the homogeneous linewidth for the erbium transition in glass at such low temperatures. It is therefore still an open question if the observations are first indications of zero-threshold behaviour, or just some less fundamental technological phenomenon [33].

One of the spectacular results of the research on DFB fibre lasers is that they can quite easily be cascaded to form multi-wavelength sources [74]. This way one pump laser can pump several DFB fibre lasers without significant loss of quality for the

individual lasers. The wavelengths of the individual lasers can be fabricated with sufficient precision that they can be readily used in a modern WDM system. Even more precise fabrication and dense packing of the wavelengths can be obtained when transferring the technology to waveguide DBR lasers [80].

Finally, it is worth mentioning that after several years of research, DFB lasers were fabricated and operated at wavelengths up to 1618nm [76]. This was obtained despite that the first theoretical estimates claimed that the limit would be around 1610nm due to problems with low gain in erbium and two-photon absorption inside the cavity. However, by using all the know-how built up during five years of research it was still possible. The output spectrum of a long-wavelength DFB laser at room temperature is shown in Fig. 16. Demonstration of this achievement completes the section about DFB fibre lasers.

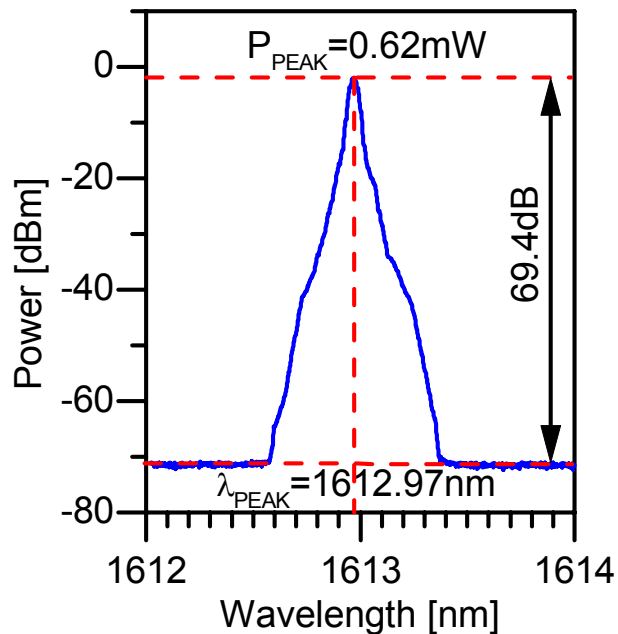


Fig. 16. Spectrum of long-wavelength DFB fibre laser recorded with an optical spectrum analyser [76]. Note that the spectral shape is entirely given by the filter function for the ANDO spectrum analyser. The 100-mm long DFB laser was pumped with 60mW at 980nm.

## Strong gratings

Fig. 17 shows an example of a 23mm long 80-dB grating written with the polarization-control method, illustrating that it is capable of producing very strong gratings without significant distortions.

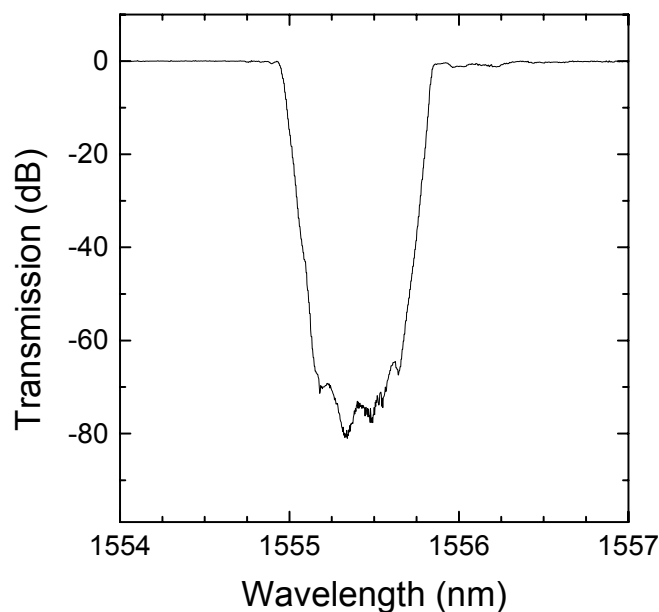


Fig. 17. A 23mm long Gaussian grating written in a deuterium-loaded HNLF fibre using a single excimer laser exposure with the polarization-control method. Notice the grating strength of more than 80dB, which is partially limited by the dynamic range of the detection system (ANDO AQ4321 laser in combination with ANDO AQ6317B spectrum analyser) [44].

## Thermal stability of gratings

In view of the commercial importance of the thermal stability of gratings one finds surprisingly few systematic experimental investigations published in the literature. One reason is that the subject is very complicated. The thermal stability of a grating depends on a large number of parameters such as the germanium concentration in the fibre core, co-dopants in the fibre, defect concentration in the fibre, the intensity of the UV laser, the strength of the grating, the exact writing method used, post annealing of the grating, etc. We have no intention to describe all these things in detail. However, we would like to give a few instructive examples.

In Fig. 18 we show the decay of the relative strength of a number of different gratings written in two different fibres during isochronal anneal. The relative strength means that the modulation strength (refractive index modulation) was normalised to 1 after the UV writing but prior to the post anneal. Generally one can see 4 interesting trends:

- 1) From room temperature up to the post anneal temperature the grating strength is almost constant.
- 2) At high temperatures gratings written in a fibre with a low germanium concentration in the core are more stable than gratings written in a fibre with a high germanium concentration.
- 3) At medium temperatures weak gratings survive better (in a relative sense) than strong gratings. Of course there is still more *absolute* modulation strength left for the strong grating.
- 4) The temperature at which the grating is completely annealed out shows a very systematic decrease with increasing germanium concentration in the core (only valid for simple gratings of type 1). This dependence was predicted by the model described in references [8,15].

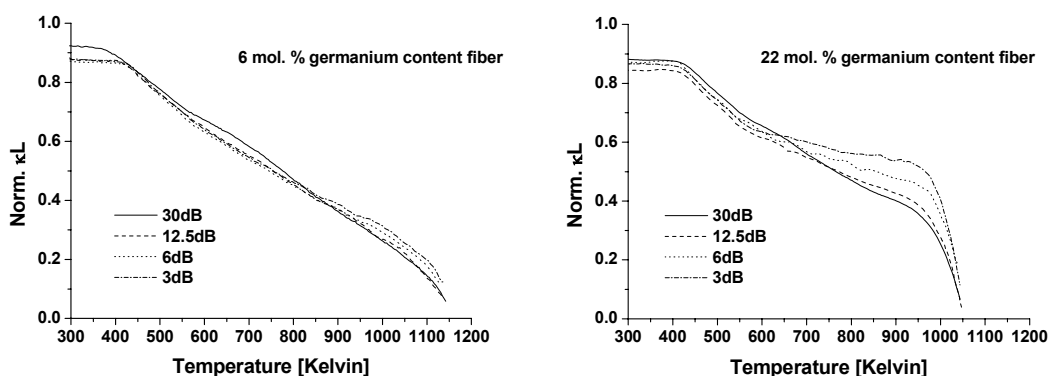


Fig. 18. A comparison of the relative thermal stability of gratings of different strengths is performed for gratings written in two different fibres with 6% germanium and 22% germanium in the core [81] with 266nm UV light. The experimental method is described in detail in reference [14].



**Professor Martin Kristensen**

*Department of Physics and Astronomy and  
Interdisciplinary Nanoscience Center (iNANO)  
University of Aarhus, Ny Munkegade, Building 1520, DK-8000 Århus C, Denmark  
E-mail: [mk@phys.au.dk](mailto:mk@phys.au.dk), telephone (+45)-89425532*

## References

- [1] K.O. Hill, Y. Fujii, D.C. Johnson and B.S. Kawasaki, 'Photosensitivity in optical fiber waveguides: Application to reflection filter fabrication', *Applied Physics Letters* **32**, 647-649 (1978)
- [2] G. Meltz, W.W. Morey and W.H. Glenn, 'Formation of Bragg gratings in optical fibers by a transverse holographic method', *Optics Letters* **14**, 823-825 (1989)
- [3] H. Hosono, Y. Abe, D.L. Kinser, R.A. Weeks, K. Muta and H. Kawazoe, 'Nature and origin of the 5-eV band in SiO<sub>2</sub>:GeO<sub>2</sub> glasses', *Physical Review B* **46**, 11445-11451 (1992)
- [4] M. Fujimaki, T. Watanabe, T. Katoh, T. Kasahara, N. Miyazaki, Y. Ohki and H. Nishikawa, 'Structures and generation mechanisms of paramagnetic centers and absorption bands responsible for Ge-doped SiO<sub>2</sub> optical-fiber gratings', *Physical Review B* **57**, 3920-3926 (1998)
- [5] L. Skuja, 'Optically active oxygen-deficiency-related centers in amorphous silicon dioxide', *Journal of Non-Crystalline Solids* **239**, 16-48 (1998)
- [6] J. Nishii, K. Kintaka, H. Hosono, H. Kawazoe, M. Kato and K. Muta, 'Pair generation of Ge electron centers and self-trapped hole centers in GeO<sub>2</sub>-SiO<sub>2</sub> glasses by KrF excimer-laser irradiation', *Physical Review B* **60**, 7166-7169 (1999)
- [7] L. Skuja, M. Hirano and H. Hosono, 'Oxygen-Related Intrinsic Defects in Glassy SiO<sub>2</sub>: Interstitial Ozone Molecules', *Physical Review Letters* **84**, 302-305 (2000)
- [8] M. Kristensen, 'Ultraviolet-light-induced processes in germanium-doped silica', *Physical Review B* **64**, article number 144201, 4201-4212 (2001)
- [9] M.G. Sceats, G.R. Atkins and S.B. Poole, 'Photolytic index changes in optical fibers', *Annual Review of Material Science* **23**, 381-410 (1993)
- [10] H.G. Limberger, P.Y. Fonjallaz, R.P. Salathé and F. Cochet, 'Compaction- and photoelastic-induced index changes in fiber Bragg gratings', *Applied Physics Letters* **68**, 3069-3071 (1996)
- [11] M. Douay, W.X. Xie, T. Taunay, P. Bernage, P. Niay, P. Cordier, B. Poumellec, L. Dong, J.F. Bayon, H. Poignant and E. Delevaque, 'Densification Involved in the UV-Based Photosensitivity of Silica Glasses and Optical Fibers', *Journal of Lightwave Technology* **15**, 1329-1342 (1997)
- [12] F. Piao, W.G. Oldham and E.E. Haller, 'The mechanism of radiation-induced compaction in vitreous silica', *Journal of Non-Crystalline Solids* **276**, 61-71 (2000)
- [13] T. Erdogan, V. Mizrahi, P.J. Lemaire and D. Monroe, 'Decay of ultraviolet-induced fiber Bragg gratings', *Journal of Applied Physics* **76**, 73-80 (1994)
- [14] J. Rathje, M. Kristensen and J.E. Pedersen, 'Continuous anneal method for characterizing the thermal stability of ultraviolet written Bragg gratings', *Journal of Applied Physics* **88**, 1050-1055 (2000)
- [15] M. Kristensen, 'Refractive Index Engineering in Silica Glass', Dr. Techn. (Habilitation) thesis, (Research Center COM, DTU, Kgs. Lyngby, Denmark, 2003)
- [16] S. Hüfner, 'Optical Spectra of Transparent Rare Earth Compounds', (Academic Press, New York, 1978)
- [17] R. Reisfeld and C.K. Jørgensen, 'Lasers and Excited States of Rare Earths', (Springer-Verlag, Berlin, 1977)
- [18] M.J. Yuen, 'Ultraviolet absorption studies of germanium silicate glasses', *Applied Optics* **21**, 136-140 (1982)

## Bragg Gratings White Paper

- [19] G. Pacchioni and R. Ferrario, 'Optical transitions and EPR properties of two-coordinated Si, Ge, Sn and related  $H(I)$ ,  $H(II)$ , and  $H(III)$  centers in pure and doped silica from *ab initio* calculations', *Physical Review B* **58**, 6090-6096 (1998)
- [20] K.O. Hill, B. Malo, F. Bilodeau, D.C. Johnson and J. Albert, 'Bragg gratings fabricated in monomode photosensitive optical fiber by UV exposure through a phase mask', *Applied Physics Letters* **62**, 1035-1037 (1993)
- [21] M. Svalgaard, C.V. Poulsen, A. Bjarklev and O. Poulsen, 'Direct UV-writing of buried single-mode channel waveguides in Ge-doped silica films', *Electronics Letters* **30**, 1401-1403 (1994)
- [22] R. Kashyap, 'Fiber Bragg Gratings', (Academic Press, San Diego, USA, 1999)
- [23] B.E. Warren, 'X-ray determination of the structure of glass', *Journal of the American Ceramic Society* **17**, 249-254 (1934)
- [24] R.L. Mozzi and B.E. Warren, 'The Structure of Vitreous Silica', *Journal of Applied Crystallography* **2**, 164-172 (1969)
- [25] M. Svalgaard, 'Ultraviolet light induced refractive index structures in germanosilica', Ph.D. thesis, supervised by M. Kristensen and O. Poulsen, (Mikroelektronik Centret, DTU, Kgs. Lyngby, Denmark, 1997)
- [26] M. Svalgaard, 'Dynamics of ultraviolet induced luminescence and fiber Bragg grating formation in the high fluence regime', *OSA Technical Digest Series* **22**, 160-163 (1995)
- [27] M. Poirier, S. Thibault, J. Lauzon and F. Ouellette, 'Dynamic and orientational behavior of UV-induced luminescence bleaching in Ge doped silica optical fiber', *Optics Letters* **18**, 870-872 (1993)
- [28] M. Kristensen, 'Model for UV-induced processes in germanium-doped silica', *DOPS-NYT* **04** (3), 6-12 (2004)
- [29] J.F. Brennan III, D. Sloan, M. May and D.L. LaBrake, 'The photosensitivity and UV-induced optical loss of silica optical fibers exposed to very high-pressure hydrogen environments', *Proceedings of SPIE* **3847**, 42-47 (1999)
- [30] J.F. Brennan III, D. Sloan, J. Dent and D.L. LaBrake, 'The behavior of silica optical fibers exposed to very high-pressure hydrogen environments', *OFC'99*, Paper ThD4, 59-61, (San Diego, California, USA, 1999)
- [31] V. Butov, K.M. Golant and A.L. Tomashuk, 'Material dispersion and spectral dependence of photorefractive effect in silica glasses for fiber optics', *Proc. Int. Congr. Glass* **2**, 53-54 (2001)
- [32] J. Canning, H.J. Deyerl, H.R. Sørensen and M. Kristensen, 'Ultraviolet-induced birefringence in hydrogen-loaded optical fiber', *Journal of Applied Physics* **97**, Article 053104 (2005)
- [33] J. Hübner, 'Index Engineering with Excimer Light', Ph.D. thesis, supervised by M. Kristensen and O. Poulsen, (Mikroelektronik Centret, DTU, Kgs. Lyngby, Denmark, 1998)
- [34] J. Hübner, M. Svalgaard, L.G. Nielsen and M. Kristensen, 'Phenomenological Model of UV-induced Bragg Grating Growth in Germanosilicate Fibers', *Photonics West 97*, Paper 2998-2, 11-21, (San Jose, California, USA, 1997)
- [35] P.E. Dyer, R.J. Farley and R. Giedl, 'Analysis of grating formation with excimer laser irradiated phase masks', *Optics Communications* **115**, 327-334 (1995)
- [36] B. Malo, D.C. Johnson, F. Bilodeau, J. Albert, and K.O. Hill, 'Single-excimer-pulse writing of fiber gratings by use of a zero-order nulled phase mask: grating spectral response and visualization of index perturbations', *Optics Letters* **18**, 1277-1279 (1993)
- [37] A. Othonos and K. Kalli, 'Fibre Bragg Gratings; Fundamentals and Applications in Telecommunications and Sensing', (Artec House, Boston, 1999)

- [38] M.J. Cole, W.H. Loh, R.I. Laming, M.N. Zervas and S. Barcelos, 'Moving fibre/phase mask-scanning beam technique for enhanced flexibility in producing fibre gratings with uniform phase mask', *Electronics Letters* **31**, 1488-1490 (1995)
- [39] M. Ibsen, M.K. Durkin, M.J. Cole and R.I. Laming, 'Optimised square passband fibre Bragg grating filter with in-band flat group delay response', *Electronics Letters* **34**, 800-802 (1998)
- [40] W.H. Loh, R.I. Laming, N. Robinson, A. Cavaciuti, F. Vaninetti, C.J. Anderson, M.N. Zervas and M.J. Cole, 'Dispersion Compensation Over Distances in Excess of 500km for 10-Gb/s Systems Using Chirped Fiber Gratings', *IEEE Photonics Technology Letters* **8**, 944-946 (1996)
- [41] M. Kristensen and J. Hübner, 'Polarization control of UV writing', USA patent application submitted May 22, IP-number WO-01/90789-A2, 37 pages 12 figures (2000)
- [42] J.B. Jensen, N. Plougmann, H.-J. Deyerl, P. Varming, J. Hübner and M. Kristensen, 'Polarization-control method for ultraviolet writing of advanced Bragg gratings', *Optics Letters* **27**, 1004-1006 (2002)
- [43] P. Varming, J.B. Jensen, N. Plougmann, M. Kristensen and J. Hübner, 'New method for fabrication of advanced UV written Bragg gratings', BGPP'01, Paper BWA5, 1-3, (Stresa, Italy, 2001)
- [44] J.B. Jensen, N. Plougmann, H.-J. Deyerl and M. Kristensen, 'Polarization controlled UV writing of Bragg gratings', OFC'02, Paper TuQ4, 111-113, (Anaheim, California, USA, 2002)
- [45] N. Plougmann, 'Advanced techniques for fabricating Bragg gratings', Master thesis, supervised by M. Kristensen, P. Varming, J.B. Jensen and H.J. Deyerl, (Research Center COM, DTU, Kgs. Lyngby, Denmark, 2001)
- [46] 'IFO\_Gratings 4.0 software', see [www.optiwave.com](http://www.optiwave.com)
- [47] M. Ibsen, P. Petropoulos, M.N. Zervas and R. Feced, 'Dispersion-free fibre Bragg gratings', OFC'01, Paper MC1, (Anaheim, California, USA, 2001)
- [48] M. Ibsen, R. Feced, J.A.J. Fells and W.S. Lee, '40Gbit/s high performance filtering for DWDM networks employing dispersion-free fibre Bragg gratings', Proceedings of ECOC'01, Paper Th.B.2.1, 594-595, (Amsterdam, Holland, 2001)
- [49] B.J. Eggleton, G. Lenz, N. Litchinitser, D.B. Patterson and R.E. Slusher, 'Implications of Fiber Grating Dispersion for WDM Communication Systems', *IEEE Photonics Technology Letters* **9**, 1403-1405 (1997)
- [50] G. Nykolak, B.J. Eggleton, G. Lenz and T.A. Strasser, 'Dispersion Penalty Measurements of Narrow Fiber Bragg Gratings at 10Gb/s', *IEEE Photonics Technology Letters* **10**, 1319-1321 (1998)
- [51] H.J. Deyerl, N. Plougmann, J.B.D. Jensen, J. El-Bez, H.R. Sørensen, C. Peucheret and M. Kristensen, 'Low-dispersion fiber Bragg gratings written using the polarization control method', ECOC'02, Paper 7.2.7, (Copenhagen, Denmark, 2002)
- [52] L. Poladian, 'Simple grating synthesis algorithm', *Optics Letters* **25**, 787-789 (2000)
- [53] W.H. Press, B.P. Flannery, S.A. Teukolsky and W.T. Vetterling, 'Numerical Recipes', (Cambridge University Press, Cambridge, England, 1989)
- [54] C.L. Lee and Y. Lai, 'Evolutionary programming synthesis of advanced fiber grating devices', CLEO/QELS'03, Paper CTu5, (Baltimore, USA, 2003)
- [55] A.V. Buryak, 'Iterative scheme for the 'mixed' scattering problem', BGPP'03, Paper MB3, 27-29, presented at the conference on 'Bragg gratings, photosensitivity and poling in glass waveguides', (Monterey, USA, 2003)
- [56] N. Plougmann and M. Kristensen, 'Efficient iterative technique for designing Bragg gratings', *Optics Letters* **29**, 23-25 (2004)
- [57] P.I. Borel, A. Harpøth, L.H. Frandsen, M. Kristensen, P. Shi, J.S. Jensen and O. Sigmund, 'Topology optimization and fabrication of photonic crystal structures', *Optics Express* **12**, 1996-2001 (2004)

## Bragg Gratings White Paper

- [58] H.J. Deyerl, N. Plougmann, J.B. Jensen, F. Floreani, H.R. Sørensen and M. Kristensen, 'Fabrication of advanced Bragg gratings with complex apodization profiles by use of the polarization control method', *Applied Optics* **43**, 3513-3522 (2004)
- [59] H.J. Deyerl, C. Peucheret, B. Zsigri, F. Floreani, N. Plougmann, S.J. Hewlett, M. Kristensen and P. Jeppesen, 'A compact low dispersion fiber Bragg grating with high detuning tolerance for advanced modulation formats', *Optics Communications* **247**, 93-100 (2005)
- [60] R. Kashyap, G.D. Maxwell and B.J. Ainslie, 'Laser-Trimmed Four-Port Bandpass Filter Fabricated in Single-Mode Photosensitive Ge-Doped Planar Waveguide', *IEEE Photonics Technology Letters* **5**, 191-194 (1993)
- [61] Y. Hibino, T. Kitagawa, K.O. Hill, F. Bilodeau, B. Malo, J. Albert and D.C. Johnson, 'Wavelength Division Multiplexer with Photoinduced Bragg Gratings Fabricated in a Planar-Lightwave-Circuit-Type Asymmetric Mach-Zehnder Interferometer on Si', *IEEE Photonics Technology Letters* **8**, 84-86 (1996)
- [62] J.-M. Jouanno, D. Zauner and M. Kristensen, 'Low crosstalk planar optical add-drop multiplexer fabricated with UV-induced Bragg gratings', *Electronics Letters* **33**, 2120-2121 (1997)
- [63] J.-P. Weber, 'Spectral characteristics of coupled-waveguide Bragg-reflection tunable optical filter', *IEE proceedings-J* **140**, 275-284 (1993)
- [64] H.H. Yaffe, C. H. Henry, M. R. Serbin and L. G. Cohen, 'Resonant Couplers Acting as Add-Drop Filters Made with Silica-on-Silicon Waveguide Technology', *Journal of Lightwave Technology* **12**, 1010-1014 (1994)
- [65] Y. Tachikawa, Y. Inoue, M. Kawachi, H. Takahashi and K. Inoue, 'Arrayed-waveguide grating add-drop multiplexer with loop-back optical paths', *Electronics Letters*, **29**, 2133-2134 (1993)
- [66] H. Venghaus, A. Gladisch, B.F. Jørgensen, J.-M. Jouanno, M. Kristensen, R.J. Pedersen, F. Testa, D. Trommer and J.P. Weber, 'Optical add/drop multiplexers for WDM communication systems', *OFC'97*, Paper Thj1, 280-281, (Dallas, Texas, USA, 1997)
- [67] D.A. Zauner, J. Hübner, K.J. Malone, and M. Kristensen, 'UV-trimming of arrayed-waveguide grating wavelength division demultiplexers', *Electronics Letters* **34**, 780-781 (1998)
- [68] P.J. Lemaire, R.M. Atkins, V. Mizrahi and W.A. Reed, 'High pressure H<sub>2</sub> loading as a technique for achieving ultrahigh UV photosensitivity and thermal sensitivity in GeO<sub>2</sub> doped optical fibres', *Electronics Letters* **29**, 1191-1193 (1993)
- [69] V. Mizrahi, D.J. DiGiovanni, R.M. Atkins, S.G. Grubb, Y.K. Park and J.M.P. Delavaux, 'Stable Single-Mode Erbium Fibre-Grating Laser for Digital Communication', *Journal of Lightwave Technology* **11**, 2021-2025 (1993)
- [70] J.T. Kringlebotn, J.-L. Archambault, L. Reekie and D.N. Payne, 'Er<sup>3+</sup>:Yb<sup>3+</sup>-codoped fiber distributed-feedback laser', *Optics Letters* **19**, 2101-2103 (1994)
- [71] J. Canning and M.G. Sceats, 'π-phase-shifted periodic distributed structures in optical fibres by UV post-processing', *Electronics Letters* **30**, 1344-1345 (1994)
- [72] W.H. Loh and R.I. Laming, '1.55μm phase-shifted distributed feedback fibre laser', *Electronics Letters* **31**, 1440-1442 (1995)
- [73] M. Sejka, P. Varming, J. Hübner and M. Kristensen, 'Distributed feedback Er<sup>3+</sup>-doped fibre laser', *Electronics Letters* **31**, 1445-1446 (1995)
- [74] J. Hübner, P. Varming and M. Kristensen, 'Five wavelength DFB fibre laser source for WDM systems', *Electronics Letters* **33**, 139-140 (1997)
- [75] P. Varming, J. Hübner and M. Kristensen, 'DFB fiber laser as source for optical communication systems', *OFC'97*, Paper WL7, 169, (Dallas, Texas, USA, 1997)

## Bragg Gratings White Paper

- [76] P. Varming, V.C. Lauridsen, J.H. Povlsen, J.B. Jensen, M. Kristensen and B. Pálsdóttir, 'Design and fabrication of Bragg grating based DFB fiber lasers operating above 1610 nm', OFC'00, Paper ThA6, 17-19, (Baltimore, USA, 2000)
- [77] J.L. Philipsen, M.O. Berendt, P. Varming, V.C. Lauridsen, J.H. Povlsen, J. Hübner, M. Kristensen and B. Pálsdóttir, 'Polarisation control of DFB fibre laser using UV-induced birefringent phase-shift', Electronics Letters 34, 678-679 (1998)
- [78] M. Kristensen, J. Hübner, P. Varming, M. Sejka and B. Pálsdóttir, 'Polarisation asymmetric active optical waveguide, method of its production, and its uses', Danish patent application number DK970168, IP-number 6151429, 42 pages 12 figures (1997)
- [79] M. Sejka, J. Hübner, P. Varming, T. Feuchter, B. Palsdottir, C.C. Larsen and M. Kristensen, 'UV-Induced DFB Laser in Ge-free Erbium Doped Fiber', CLEO/Europe, Paper CThG3, 248, (Hamburg, Germany, 1996)
- [80] S. Guldberg-Kjær, J. Hübner, M. Kristensen, C. Laurent-Lund, M.R. Poulsen and M.W. Sckerl, 'Planar waveguide laser in Er/Al-doped germanosilicate', Electronics Letters 35, 302-303 (1999)
- [81] H.J. Deyerl, H.R. Sørensen, J.B.D. Jensen, N. Plougmann and M. Kristensen, 'Fabrication and stability of fiber Bragg gratings for WDM applications using a 266nm cw laser', Paper CTuI2, CLEO/QELS'03, (Baltimore, USA, 2003)